

Article

Assessment of Air Pollution Levels during Sugarcane Stubble Burning Event in La Feria, South Texas, USA

Sai Deepak Pinakana, Edward Robles, Esmeralda Mendez and Amit U. Raysoni * 

School of Earth, Environmental and Marine Sciences, The University of Texas Rio Grande Valley, Brownsville, TX 78520, USA

* Correspondence: amit.raysoni@utrgv.edu

Abstract: Agricultural stubble burning is the third largest source of air pollution after vehicular and industrial emissions. Fine particulate matter (PM_{2.5}), volatile organic compounds (VOCs), carbon monoxide (CO), nitrogen dioxide (NO₂), and black carbon (BC) are some of the pollutants emitted during such burning events. The Lower Rio Grande Valley (RGV) region of South Texas is a major hub of agricultural activity, and sugarcane farming is one of them. Unfortunately, this activity results in episodic events of high air pollution in this low-resourced, Hispanic/Latino majority region of the U.S.–Mexico border. This study presents results from a sugarcane site in La Feria, South Texas, where the air quality was monitored before, during, and after the sugarcane stubble burning. Various parameters were monitored on an hourly basis from 24 February 2022 to 4 April 2022. Our results demonstrate high levels of all the monitored pollutants during the burning phase in contrast to the pre- and post-burning period. The black carbon levels went up to 6.43 μg m⁻³ on the day of burning activity. An increase of 10%, 11.6%, 25.29%, 55%, and 67.57% was recorded in the PM₁, PM_{2.5}, PM₁₀, Black Carbon, and CO levels, respectively, during the burning period in comparison with the total study period. The absorption Ångström exponent value reached a maximum value of 2.03 during the burning activity. The PM_{2.5}/PM₁₀ ratio was 0.87 during the burning activity. This study also highlights the importance for continuous monitoring of air quality levels due to stubble burning in the Lower Rio Grande Valley Region of South Texas.



Citation: Pinakana, S.D.; Robles, E.; Mendez, E.; Raysoni, A.U.

Assessment of Air Pollution Levels during Sugarcane Stubble Burning Event in La Feria, South Texas, USA. *Pollutants* **2023**, *3*, 197–219. <https://doi.org/10.3390/pollutants3020015>

Academic Editors: Enrico Ferrero and Elvira Kovač-Andrić

Received: 17 January 2023

Revised: 6 February 2023

Accepted: 17 March 2023

Published: 24 March 2023



Copyright: © 2023 by the authors. Licensee MDPI, Basel, Switzerland. This article is an open access article distributed under the terms and conditions of the Creative Commons Attribution (CC BY) license (<https://creativecommons.org/licenses/by/4.0/>).

Keywords: stubble burning; PM_{2.5}; sugarcane; Rio Grande Valley; South Texas; black carbon; absorption angstrom exponent

1. Introduction

Stubble burning is the phenomenon which involves burning the crop residue pre- and post-harvest season to prepare the fields for planting. While pre-harvest burning is conducted to control the weeds and pests, post-harvest season involves in burning stubble which consists of stalks leftover after harvest [1]. This process is also called crop residue burning or agricultural burning. Even though there are productive ways to use the stubble, farmers consider burning as the best method to remove residues because of its cost-friendly nature and involvement of minimum labor and time [2]. Various alternate ways in which the stubble can be used include residue in biothermal power plants and the production of biogas, paper, and bedding material for cattle [3].

Stubble burning is the leading source of air pollution and stands only after vehicular and industrial emissions [4]. Countries including India, Pakistan, Australia, the United States, and New Zealand are some of the most affected by stubble burning [5]. The burning of the residue leads to the emission of various air pollutants, which includes ammonia (NH₃), carbon monoxide (CO), carbon dioxide (CO₂), sulfur dioxide (SO₂), oxides of nitrogen (NO_x), volatile organic carbon (VOC), and particulate matter (PM_{2.5}, PM₁₀) [6]. These pollutants not only harm environmental air quality but continuous exposure to pollutants such as PM_{2.5} leads to respiratory and cardiovascular diseases in

human beings [7]. Ammonia emissions have a significant impact on the formation of particulate matter and ground-level ozone, which can harm human health and damage crops and other vegetation [8]. Carbon monoxide (CO) is a toxic gas that can reduce oxygen delivery to the body's organs and tissues and can also contribute to the formation of ground-level ozone [9]. According to the United States Environmental Protection Agency (EPA), carbon monoxide is a leading cause of air pollution-related illness and death [10]. The gas is primarily produced by the burning of fossil fuels and is found in the exhaust emissions of vehicles, power plants, and other industrial sources. Sulfur dioxide (SO₂) is a major contributor to acid rain, which can harm plants, animals, and bodies of water. According to the EPA, SO₂ emissions primarily come from the burning of fossil fuels in power plants and industrial facilities [11]. Oxides of nitrogen (NO_x) emissions from transportation and other sources have increased in the United States by approximately 7% since 1990 [12]. Continuous exposure to PM_{2.5} can have both short-term and long-term effects on human health [7].

Major crops such as wheat, rice, maize, cotton, and sugarcane are some of the most burnt residues across the world. A study published in 2018 analyzed the data of air pollutants emitted due to stubble burning of maize and concluded that CO₂ is the highest of all emissions, followed by CO, PM₁₀, PM_{2.5}, and others [13]. India, one of the largest producers of rice and wheat, produces approximately 620 million tonnes of crop residue in total. The residue generated in India can be used to generate up to 18,000 MW of electricity, whereas nearly 62% of the residue is burnt openly [14]. A study estimated that burning 1 tonne of rice residue results in the release of 29 lb particulate matter, 132 lb CO, 3218 lb CO₂, 7.7 lb NO_x, and 0.4 lb SO₂ [15].

The United States of America comprises 40% of its land area, i.e., 900.2 million acres out of 2250 million acres as agricultural land, which is the highest compared to other countries in terms of area [16]. Some of the major crops cultivated in the USA include corn, soybeans, barley, oats, rice, sugarcane, and cotton [17]. Sugarcane is primarily harvested in Florida, Louisiana, and Texas [17]. Because of its subtropical climatic features, the southern tip of the state, otherwise called Rio Grande Valley, is the largest producer of sugarcane in Texas [18]. The harvest area is 36,100 acres and produces over 143,000 short tons, raw value (STRV) [18]. The sugarcane plant has 2 parts, the first, which is net cane/stalk, is used to extract or crystallize sugar and covers 75–80% of the plant. The other 20–25% of the plant is made up of leafy matter that serves no purpose. Typically, the portion of 20–25% is the part that is burned. Even though burning would clear only one-half to two-thirds of the total residue, farmers consider that as the best option because other methods, which include transportation and processing, would cost approximately USD 24 million [19]. A study [20] in Brazil concluded that the emission factors in grams for one kg of burned dry biomass are 1303 ± 218 for CO₂, 65 ± 14 for CO, 1.5 ± 0.4 for NO_x, and 2.6 ± 1.6 for PM_{2.5}. A study [21] in Argentina inferred that there is an increased nitrous oxide (N₂O) concentration noticed from the stubble burning of sugarcane which used nitrogen fertilizers. Nitrogen is widely used to achieve maximum yields of sugarcane as it is a biomass-producing crop [22]. Additionally, it is very important to monitor the stubble burning of agriculture because N₂O is one of the greenhouse gases. There was an increase of 14% in annual emissions of N₂O from 1990 to 2020 [23].

The Rio Grande Valley, despite being one of the major producers of sugarcane in the United States of America, does not have many studies which analyze its air quality deterioration of air quality parameters due to stubble burning of sugarcane. This study presents the analysis of various air quality parameters, which include PM_{2.5}, CO, NO₂, O₃, and BC, during a stubble burn at a sugarcane site in La Feria, South Texas, TX, USA. There are only five Texas Commission on Environmental Quality (TCEQ) [24] continuous ambient monitoring station (CAMS) sites in the region of Rio Grande Valley, and not all of them measure the major USEPA criteria air pollutants. Thus, it is imperative to study the effects of stubble burning on air quality in the region. The air quality parameters were monitored using the in situ sensors at the site, and meteorological data was collected from the Texas

Commission on Environmental Quality (TCEQ) [24] continuous ambient monitoring station (CAMS) sites for the study period.

2. Study Design and Methods

2.1. Site Selection

Texas, being the third highest sugarcane producer in the United States, Rio Grande Valley, owns approximately 16,916 Ha of land dedicated to sugarcane production [25]. This study focuses on one of those sugarcane sites located in the Lower Rio Grande Valley at La Feria. The site is located 2.7 miles northwest of the La Feria residential area, 1.7 miles north of the E Interstate Highway 2, and 3.53 miles northwest of La Feria Reservoir. Sharing its boundaries with a ranch to the east and sites in the other directions, it covers 15.83 Ha of the area and is square in shape with a perimeter of 5255 ft. Regular activities, such as BBQ/Cigar, were also conducted at the site during the study period as part of home maintenance. The study period lasted from 4 February 2022 to 4 April 2022.

Additionally, data from nearby CAMS sites in Rio Grande Valley were collected to complete the required analysis. The site and Texas Commission on Environmental Quality (TCEQ) continuous air monitoring sites (CAMS) are illustrated in Figure 1.

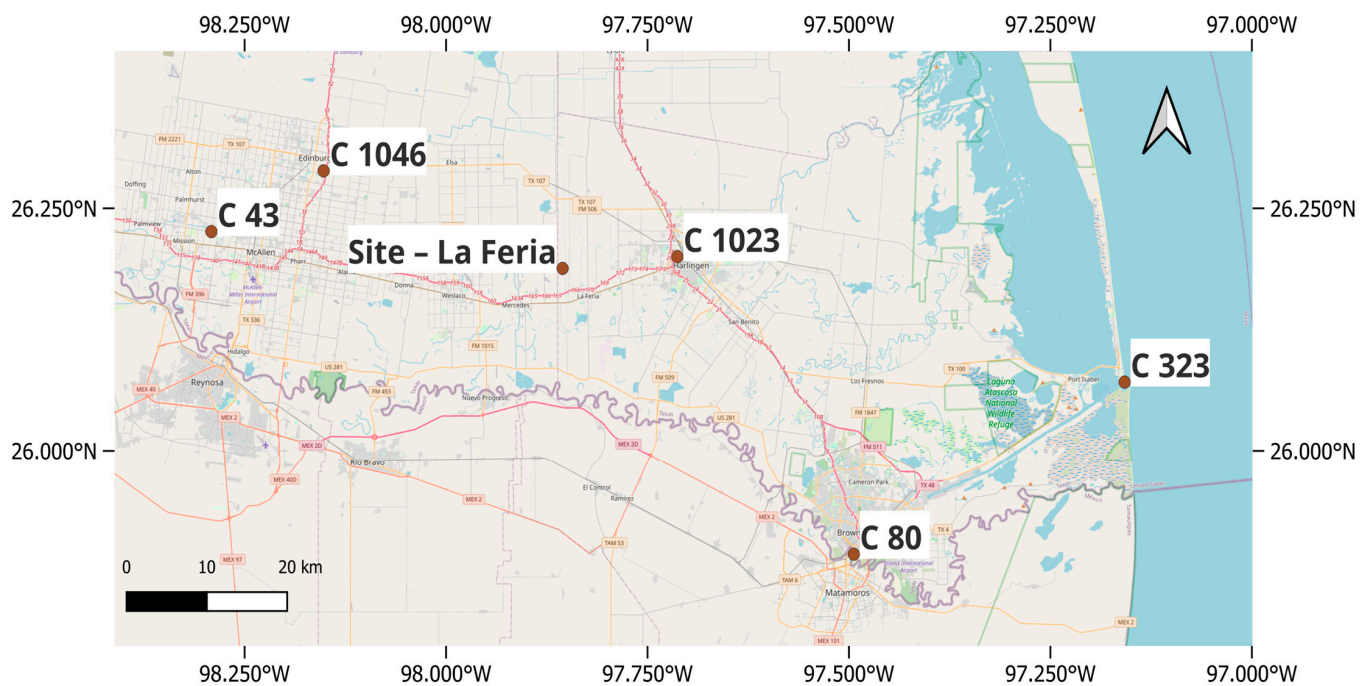


Figure 1. Map of the study location showing the study site and TCEQ CAMS sites.

2.2. Topography and Meteorological Conditions

Wind patterns from 24 February 2022 to 4 April 2022 of all the five TCEQ CAMS, i.e., C80, C1023, C323, C43, and C1046, are visualized with the help of wind rose plots in Figure 2. Averaged wind speeds of the stations were as follows: C80 (3.48 ms^{-1}), C1023 (4.14 ms^{-1}), C323 (2.94 ms^{-1}), C43 (3.27 ms^{-1}), and C1046 (3.14 ms^{-1}), and direction was mostly south-eastern for the study period.

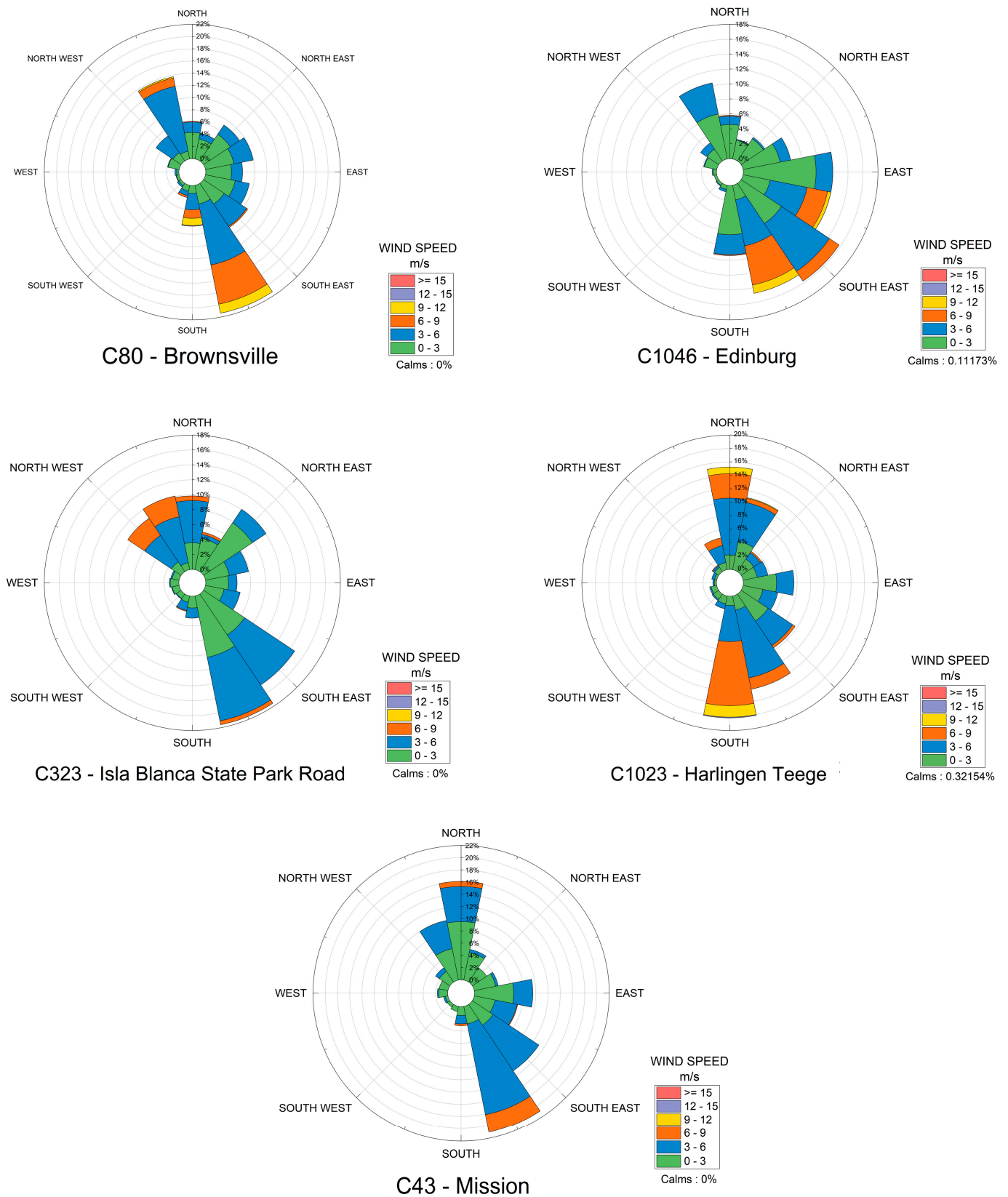


Figure 2. Wind rose diagrams for the RGV CAMSs C80, C1046, C323, C1023, and C43 during the study duration.

Meteorological parameters from the five TCEQ CAMS in the Lower RGV region (C80, C1023, C323, C43, and C1046) are summarized in Table 1 for the study period. Meteorological data from all CAMS’s was included to facilitate the analyses. The solar radiation expressed the total electromagnetic radiation at sites C80 (1.48) and C1046 (1.39) in Langley’s per minute.

Table 1. Summary statistics of 24 h meteorological parameters from CAMSs.

	Site	N	Mean	StDev	Min	Max
RWS (ms ⁻¹)	C80	932	3.48	2.31	0.04	12.29
	C1046	956	3.14	1.62	0.9	8.002
	C323	956	2.94	2.29	0	11.31
	C1023	956	4.14	2.33	0	12.15
	C46	955	3.27	1.67	0.04	8.27
T (°C)	C80	943	18.35	6.22	4.11	30.94
	C1046	956	18.65	7.41	3.16	34.77
	C323	955	17.35	4.30	6.16	26.77
	C1023	947	17.79	8.18	2.88	33.77
	C46	956	18.69	7.33	3.22	34.33
SR	C80	944	0.28	0.43	0	1.48
	C1046	956	0.28	0.42	0	1.39

StDev = standard deviation, RWS = resultant wind speed in m/s, T = temperature in (°C), and SR = solar radiation measured in Langley’s per minute.

The mean temperatures for the CAMS sites were recorded as 18.35 °C ± 6.22, 18.65 °C ± 7.41, 17.35 °C ± 4.30, 17.79 °C ± 8.18, and 18.69 °C ± 7.33 in C80, C1046, C323, C1023, and C46, respectively. There was not much difference in the mean temperatures as all the CAMS stations are from Rio Grande Valley.

2.3. Instrumentation

The instrumentation setup was on the eastern side of the field. The study period started on 24 February 2022 and continued until 4 April 2022. Various sensors were used to measure the air quality parameters during the study period. Figure 3 shows the location of the site, which was monitored, and the instrumental setup near the field.



Figure 3. Site and instrumentation setup.

DustTrak™ DRX Aerosol Monitor TSI Inc., Shoreview, MN, USA (Model:8534) was used in this study to monitor the particulate matter data. The data includes PM₁, PM_{2.5}, respirable, PM₁₀, and Total. Black carbon was measured using microAeth® MA200; AethLabs, San Francisco, CA, USA. CO and temperature were measured using Q-Trak™ Indoor Air Quality Monitor 7575 (TSI Inc., Shoreview, MN, USA). Ozone was measured using Monitor 202 (2B Technologies, Boulder, CO, USA). NO₂ was measured using 405 nm NO₂/NO/NO_x Monitor™ (2B Technologies, Inc., Boulder, CO, USA). All the concentrations were collected at 5 min intervals and converted into hourly and daily concentrations for the analysis. The data for the air quality parameters for each CAMS site were collected for the study period. All CAMS site parameters are described in Table 2.

Table 2. TCEQ CAMS site monitored parameters.

Site	C80	C1046	C323	C1023	C43
PM ₁					
PM _{2.5}	x		x		x
Resp PM					
PM ₁₀					
Total PM					
BC					
O ₃				x	x
NO ₂					
RWS	x	x	x	x	x
RWD	x	x	x	x	x
T	x	x	x	x	x
SR	x	x			

RWS = resultant wind speed in ms⁻¹, RWD = resultant wind direction in degrees, T = temperature in (°C), and SR = solar radiation measured in Langley's per minute.

2.4. Statistical Data Analysis

Descriptive statistics of the collected data were performed using Microsoft Excel (v.16.06, Microsoft Inc., Redmond, WA, USA), Origin Pro Origin Lab Corporation, Northampton, MA, USA (Version 2022). While Microsoft Excel was used to calculate the COD values and clean data, Origin Pro was used to perform Spearman correlation. Wind roses and time series graphs were also plotted using Origin Pro.

Spearman correlation was computed to signify site-specific temporal relationships with pollutant correlations at every air site. The Coefficient of Divergence (COD) was calculated to understand the spatial variation in PM_{2.5}, O₃, and temperature levels between study site and the five CAMS sites. COD specifies uniformity between two simultaneously sampled sites and is outlined as

$$COD_{j,k} = \sqrt{\frac{1}{p} \sum_{i=1}^p \left[\frac{x_{ij} - x_{ik}}{x_{ij} + x_{ik}} \right]^2}$$

where x_{ij} is the i th concentration measured at site j over the sampling period; j and k are two simultaneously sample sites; and p is the number of observations [26]. A low COD value of <0.20 denotes similar pollutant concentrations between two sites, whereas a value approaching unity indicates a significant difference in the absolute concentrations and subsequent spatial non-uniformity between the two sites. The time series were plotted to compare the values of the parameters at various times of the study period.

3. Results

3.1. 1 h Concentration Analysis

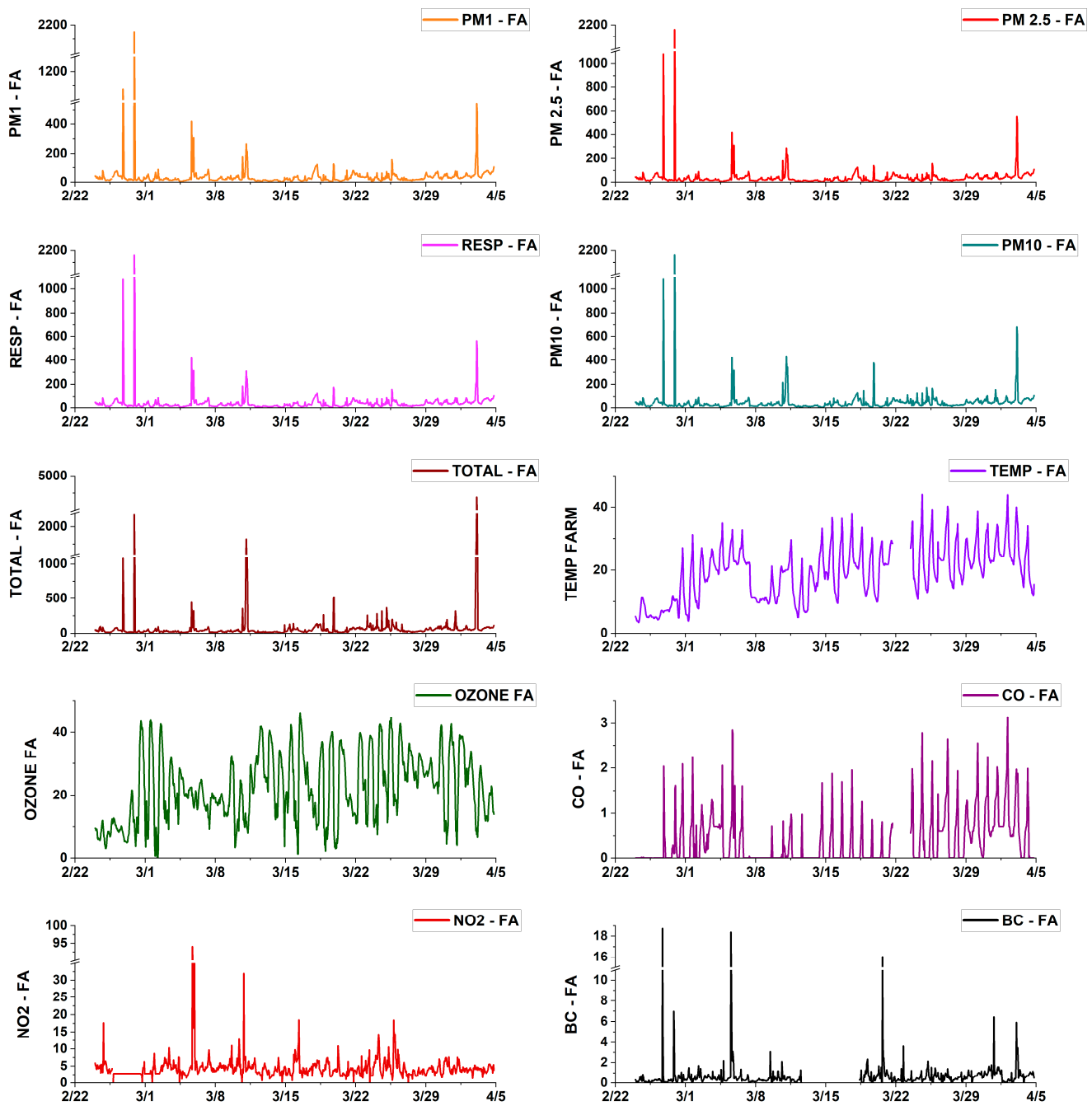
Temporal variations and descriptive statistics of all the parameters, including PM species, CO, NO₂, BC, and temperature at the site as well as the TCEQ CAMS sites in Rio Grande Valley, are presented as hourly concentrations in Table 3.

Table 3. Hourly basic statistics for various parameters at the study site and five CAMS sites.

Parameter	Location	N	Mean	StDev	Min	Max
PM ₁ (µg m ⁻³)	Site	955	39.36	93.80	1.33	2152.5
	Site	955	40.60	94.48	1.58	2161.75
PM _{2.5} (µg m ⁻³)	C80	936	7.86	6.41	0	58
	C323	953	10.86	7.91	0	60.7
	C43	868	10.21	7.89	0	52
Resp (µg m ⁻³)	Site	955	41.90	94.86	1.75	2161.83
PM ₁₀ (µg m ⁻³)	Site	955	47.85	99.47	2.58	2164.41
Total (µg m ⁻³)	Site	955	76.075	253.27	6	4690
BC (µg m ⁻³)	Site	818	0.64	1.27	0	18.74
	Site	956	22.23	10.84	0	46.20
O ₃ (ppb)	C43	944	31.62	12.92	2	68
	C1023	927	30.18	13.09	0	59
NO ₂ (ppb)	Site	955	4.46	4.27	0	94.00
CO (ppm)	Site	913	0.37	0.55	0	3.14
T (°C)	Site	955	17.61	11.16	3.40	44.07

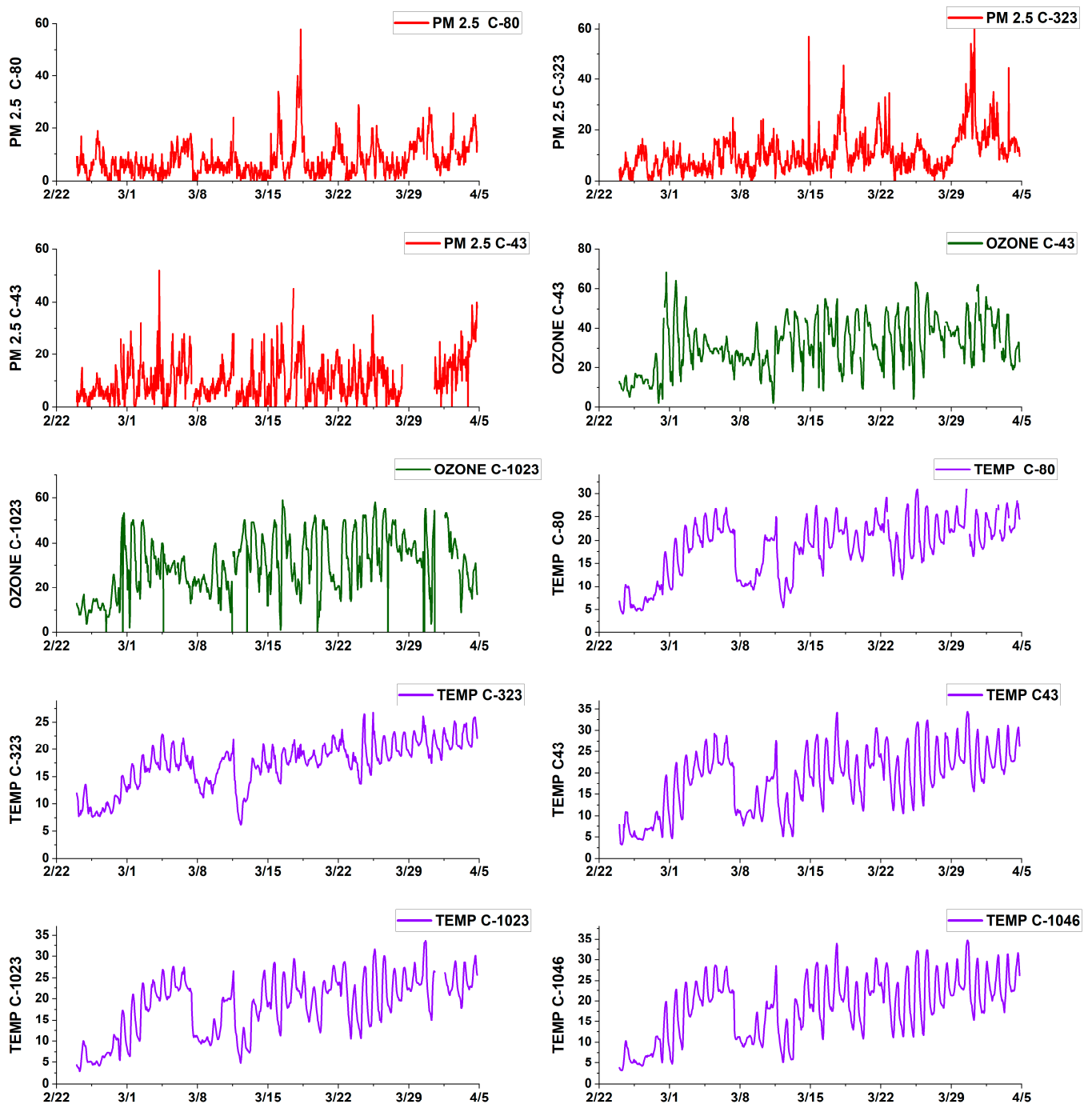
The mean (SD) of PM_{2.5} concentration for the site was $40.60 \pm 94.48 \mu\text{g m}^{-3}$ during the study period, while the CAMS sites C80, C323, and C43 recorded an average of $7.86 \pm 6.41 \mu\text{g m}^{-3}$, $10.86 \pm 7.91 \mu\text{g m}^{-3}$, and $10.21 \pm 7.89 \mu\text{g m}^{-3}$, respectively. A similar increase at the site was observed for other particulate matter sizes, including PM₁, resp, PM₁₀, and total concentrations whose mean (SD) values were recorded as $39.36 \pm 93.80 \mu\text{g m}^{-3}$, $41.90 \pm 94.86 \mu\text{g m}^{-3}$, $47.85 \pm 99.47 \mu\text{g m}^{-3}$, and $76.07 \pm 253.27 \mu\text{g m}^{-3}$, respectively. The mean (SD) ozone concentration of the site was recorded as 22.23 ± 10.84 ppb. Additionally, the same for CAMS sites C43 and C1023 was recorded as 31.62 ± 12.92 ppb and 30.18 ± 13.09 ppb, respectively. The ozone concentrations at CAMS sites were relatively higher than that of the site because of their location.

The time series of all the observed concentrations along the study period at the site and CAMS sites were plotted in Figure 4a,b, respectively. The dates and parameters are labeled appropriately on each time series to directly portray the temporal variations. The time series aid in understanding the temporal pattern during the study period. Diurnal patterns were observed for O₃, CO, and temperature values at all observed sites, as there is a difference between values in the day and night daily. BC values for the site are not present in the graph as the instrument ran out of tape from 12 March to 18 March 2022. Some hour periods were noticed to have high PM concentrations for a short period of time. As the data is collected at a site near a regular home, activities such as cigar smoking and barbecuing caused an increase in the values for a short period of time. Table 4 shows all those types of home activities at various periods in the study time, which caused an increase in the particulate matter for a short period of time.



(a)

Figure 4. Cont.



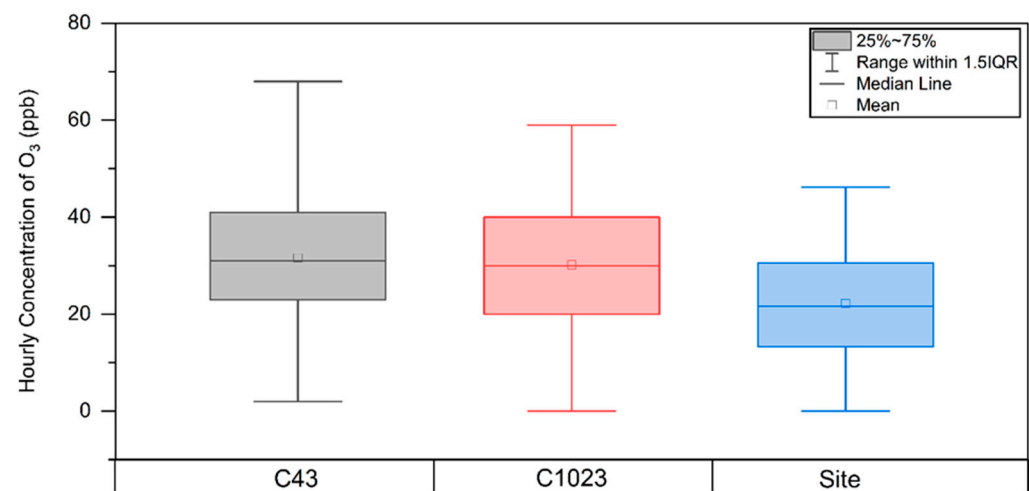
(b)

Figure 4. (a) Hourly time series of parameters at the site for the study period. (b) Hourly time series of parameters at CAMS for the study period.

Table 4. Various activities at different periods of study period, which caused a short-term increase in PM concentrations.

Date	Time	Activity
24 February 2022	18:40	cigar smoking
26 February 2022	12:55	BBQ
26 February 2022	18:45	BBQ
27 February 2022	22:15	BBQ
3 March 2022	12:40	BBQ
4 March 2022	00:50	cigar smoking
5 March 2022	18:28	BBQ
10 March 2022	18:05	cigar smoking
10 March 2022	19:15	BBQ
10 March 2022	23:00	cigar smoking
17 March 2022	22:30	cigar smoking
18 March 2022	3:25	cigar smoking
22 March 2022		Fire at Near farm

Figures 5 and 6 display the box plots for O_3 and $PM_{2.5}$, respectively. The boxes are the interquartile ranges (75th and 25th). The median is indicated by the median line inside the boxes, and the mean is indicated by the square. The outliers are not included in the boxplots. The boxplot of $PM_{2.5}$ suggests that the particulate matter concentration at the site is higher than the CAMS. Additionally, the boxplot for ozone is vice versa. The ozone concentration at the site was lower than the other two observed CAMS, i.e., C43 and C1023.

**Figure 5.** Boxplots for hourly average concentrations of O_3 (ppb) at various TCEQ CAMS sites and study site.

3.2. Coefficient of Divergence Analysis

Ambient exposure to $PM_{2.5}$, O_3 , and temperature between the site and CAMS site was calculated into COD values and are presented in Table 5. The value of COD indicates the similarity in spatial heterogeneity and concentrations, where a value less than 0.20 indicates high similarity and a value more than 0.20 shows low similarity. According to Table 5 less similarity is observed as all the values are more than 0.20. The highest COD value observed was between the site to C323 (0.647) and C80 (0.651), which indicates significant differences between the $PM_{2.5}$ values at both sites. Temperatures at all the CAMS indicate the highest similarity, as the COD values are less than 0.30. As all the observed sites are in uniform weather, a high similarity in temperatures is observed.

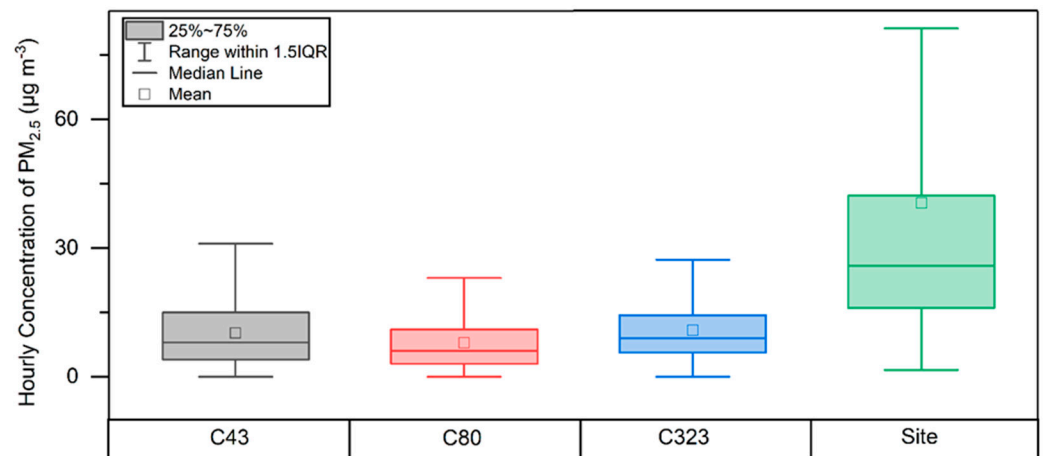


Figure 6. Boxplots for hourly average concentrations of PM_{2.5} (µg m⁻³) at various TCEQ CAMS and study site.

Table 5. COD values for the various parameters between the study site and the various CAMS sites.

Site	Parameter	CAMS	COD Value
SITE	PM _{2.5}	C80	0.651
		C43	0.544
		C323	0.647
	O ₃	C43	0.284
		C1023	0.307
		C80	0.245
	TEMPERATURE	C323	0.228
		C43	0.221
		C1023	0.269
		C1046	0.221

3.3. Spearman Correlation Coefficient Analysis

A Spearman correlation coefficients analysis was performed to study the temporal relationships between various parameters at the site and each of the CAMS. Spearman correlation is a statistical measure of the strength of the monotonic relationship between paired data. The closer the value to +1, the stronger the monotonic relationship. The Spearman correlation coefficient for this study is presented in Figure 7. The color coordination for the COD values is as follows: dark green for a high positive relationship, light green for a low positive relationship, white for no relationship, light red for a low negative relationship, and dark red for a high negative relationship.

Different particulate matter concentrations at the site are highly correlated with each other ($r \geq 0.9$). Ozone at all the observed stations is moderately correlated with the temperature at the CAMS and the site ($0.4 < r < 0.6$). NO₂ observed at the site has a weak negative correlation with the temperature at both CAMS and the site ($0 < r < -0.1$). Ozone at all observed sites is negatively correlated to PM₁, PM_{2.5}, respirable, PM₁₀, and total concentrations at the site ($0 < r < -0.4$).

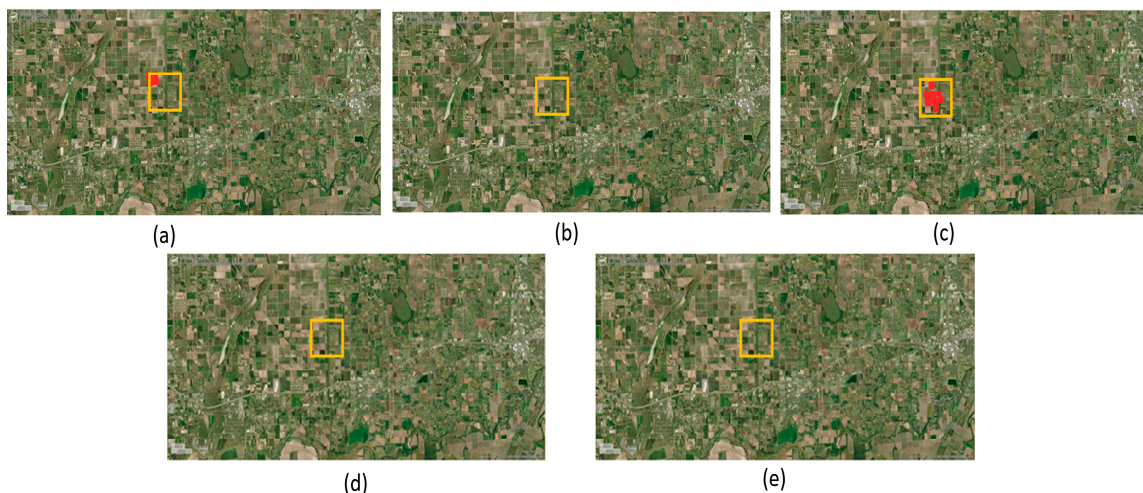


Figure 8. FIRMS US/CANADA images of the site on (a) 22 March, (b) 30 March, (c) 31 March, (d) 1 April, and (e) 2 April.

The air quality parameters recorded a step increase in their concentrations during the burning period. However, as there were some activities which caused the short-term increase in the concentrations, the effect of stubble burning could not be clearly visualized in Figure 4a. For a clear understanding of the stubble burning on air quality, Figures 9–11 visualize different parameters at the site in the range of 1 week from the burning activity. No other activity, including BBQ/cigar smoking, which would possibly cause an increase in the concentrations, took place during this one week.

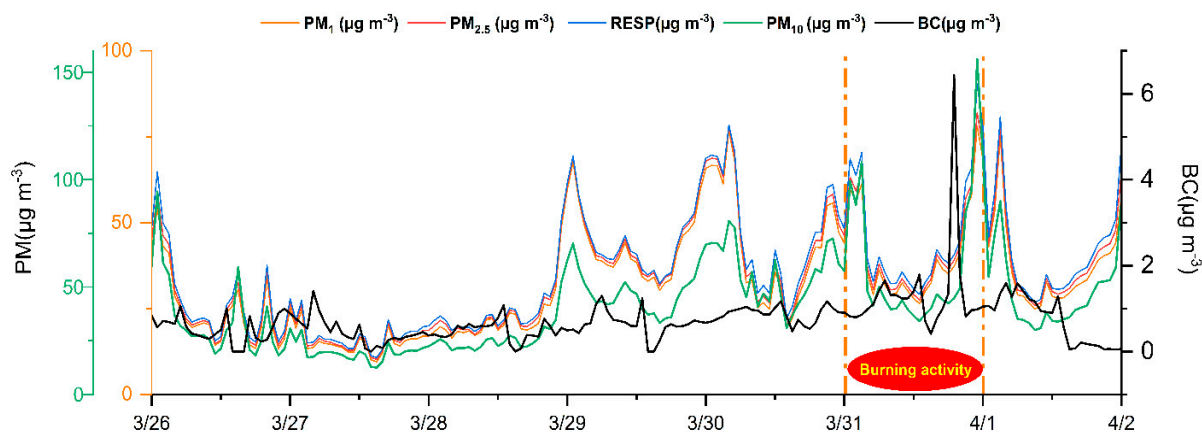


Figure 9. Hourly time series of PM and BC at the site.

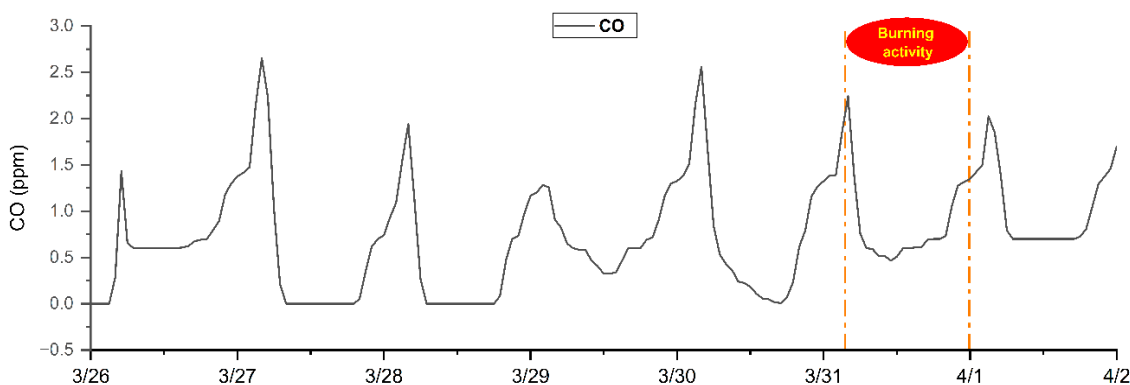


Figure 10. Hourly time series of CO at the site.

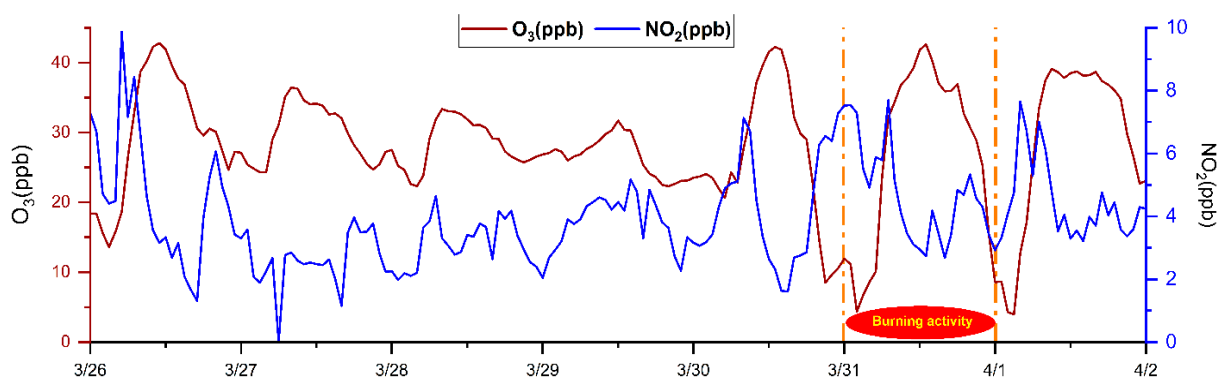


Figure 11. Hourly time series of O_3 and NO_2 at the site.

Hourly concentrations of PM_{10} , $PM_{2.5}$, respirable, PM_{10} , and black carbon for the range of 1 week from the burning activity are presented in Figure 9. The mean PM_{10} concentration for the site before the burning activity was $36.31 \pm 96.48 \mu g m^{-3}$, and during the day of burning activity was $40.44 \pm 13.54 \mu g m^{-3}$. During the burning activity, there was an increase of 10% in PM_{10} concentrations compared to the mean concentration of the study period in the site, while the highest concentration recorded is $78.16 \mu g m^{-3}$. The mean $PM_{2.5}$ concentration for the site, pre-burning activity was $37.43 \pm 97.09 \mu g m^{-3}$, while the same during the day of burning activity was $42.37 \pm 14.38 \mu g m^{-3}$. During the burning activity, there was an increase of 11.6% in $PM_{2.5}$ concentrations compared to the mean concentration of the study period, while the highest concentration recorded is $82 \mu g m^{-3}$. The mean PM_{10} concentration of the site is $44 \pm 100.49 \mu g m^{-3}$ for the study period before burning activity, while during the activity, the mean was recorded as $58.82 \pm 30.41 \mu g m^{-3}$. The increase in concentrations is 25.19% compared to the mean concentration of the study period, and the highest concentration recorded during the burning activity is $156.08 \mu g m^{-3}$. Black carbon was observed to be affected by the burning with an increase of 55% compared to the mean concentration of the study period. While the mean concentration of black carbon was $0.60 \pm 1.32 \mu g m^{-3}$ for the period before the burning activity, it increased to $1.33 \pm 1.14 \mu g m^{-3}$ during the burning activity. The highest value of black carbon concentration recorded on the day of burning activity was $6.43 \mu g m^{-3}$.

Hourly concentrations of CO are presented in Figure 10. The values of CO can be observed to follow the diurnal pattern. The mean CO concentration for the site, pre-burning activity was 0.30 ± 0.50 ppm, while the same during the day of burning activity was 0.93 ± 0.47 ppm. During the burning activity, there was an increase of 67.57% in carbon monoxide concentrations compared to the mean concentration of the study period, while the highest concentration recorded is 2.2 ppm.

Hourly concentrations of O_3 and NO_2 for the range of 1 week from the burning activity are presented in Figure 11. While NO_2 increased by 5.85% from the pre-burning activity period, O_3 increased by 19.86% compared to the mean concentration of the study period. The highest concentrations of O_3 and NO_2 on the day of burning activity are 42.625 ppb and 7.7 ppb, respectively.

3.5. Relationship between $PM_{2.5}$ and PM_{10}

Particulate matter of different sizes have their own physical and chemical characteristics, which, if analyzed, gives important information about aerosol pollution, such as the cause of pollution or impact on health [28]. In order to fully understand the relationship between $PM_{2.5}$ and PM_{10} , the linear correlation and the ratio of $PM_{2.5}$ to PM_{10} for both the study period and the week of activity are shown in Figure 12a,b, respectively.

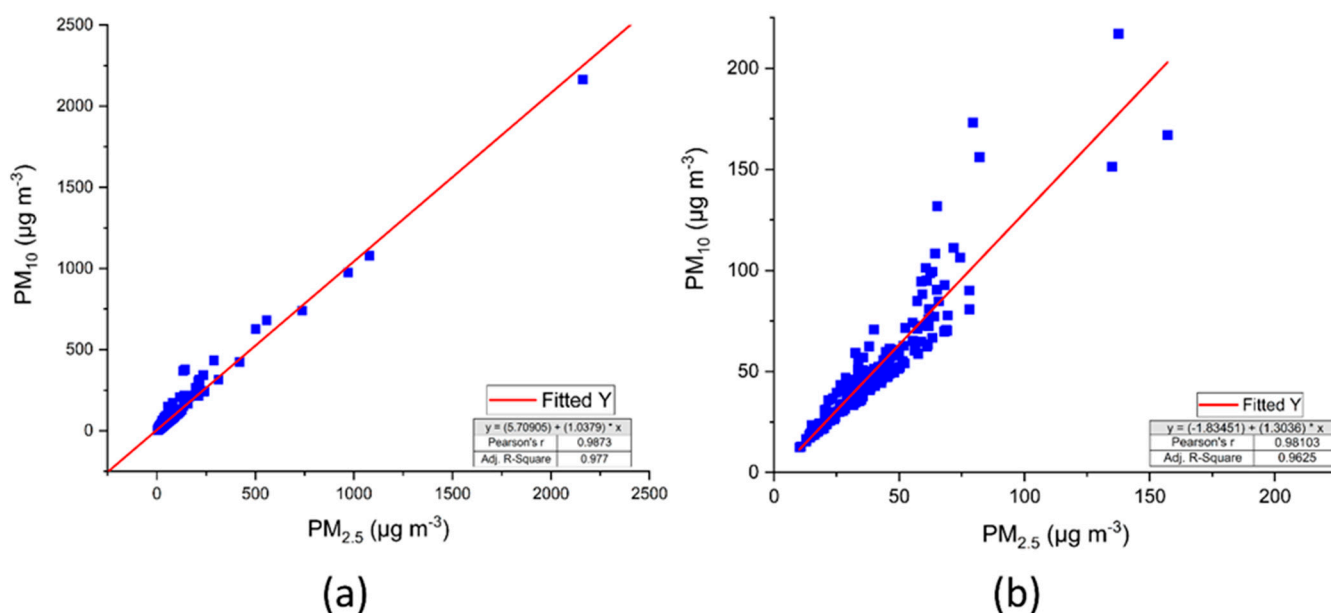


Figure 12. The regression curve of $PM_{2.5}$ and PM_{10} mass concentration for (a) study period and (b) the week of activity.

Figure 12a shows the linear correlation between $PM_{2.5}$ and PM_{10} for the whole study period while Figure 12b shows the linear correlation for the week of activity. The correlation coefficient in both cases reached $R^2 = 0.97$ and $R^2 = 0.96$, respectively, which indicates a strong correlation. The corresponding regression equations are $y = 1.0379x + 5.70905$ and $y = 1.3036x - 1.83451$, respectively. The Pearson correlation coefficient is 0.9873 and 0.9810 for the whole study period and for the week of activity, respectively, which strengthens the statement that $PM_{2.5}$ and PM_{10} are highly correlated with each other.

Values of the $PM_{2.5}/PM_{10}$ ratio have been used in previous studies to classify the type or cause of pollution [29,30]. While a lower value of $PM_{2.5}/PM_{10}$ ratio indicates the presence of more coarse particles, which is mostly caused by natural sources, a higher $PM_{2.5}/PM_{10}$ ratio indicates the cause as an anthropogenic source. Figure 13a,b show the $PM_{2.5}/PM_{10}$ ratio plots for the study period and the week of activity, respectively.

Figure 13a shows the $PM_{2.5}/PM_{10}$ ratio plots across the study period. The mean $PM_{2.5}/PM_{10}$ ratio value for the study period is 0.85 ± 0.12 . Figure 13b shows the $PM_{2.5}/PM_{10}$ ratio for the week of activity. The ratio value at the start of the day on which the burning activity took place was 0.59 and increased to 0.77 at 04:00 a.m. and then to 0.87 by 16:00 p.m. The value dropped to 0.67 at 21:00 PM on the same day. These values suggest that the $PM_{2.5}/PM_{10}$ ratios are useful in classifying the cause of the pollution as either natural or anthropogenic.

3.6. Absorption Angstrom Exponent

AAE—The absorption Ångström exponent is an aerosol optical parameter which is widely used for characterization and apportionment studies of aerosols [31]. It is calculated by using two different wavelengths. The instrument used in this study to measure black carbon is microAeth[®] MA200. This instrument measures the rate of decrease in transmitted light through the sample filter using 5 different wavelengths (880 nm, 625 nm, 528 nm, 470 nm, and 375 nm). Figure 14a,b show the measured values for different wavelengths at the site throughout the study period and during the week of burning activity, respectively. While the measurements at 880 nm and 375 nm are presented as concentrations of black carbon and UVPM ultraviolet particulate matter, respectively, measurements at other wavelengths are used to calculate the Ångström exponent for various atmospheric investigations [32].

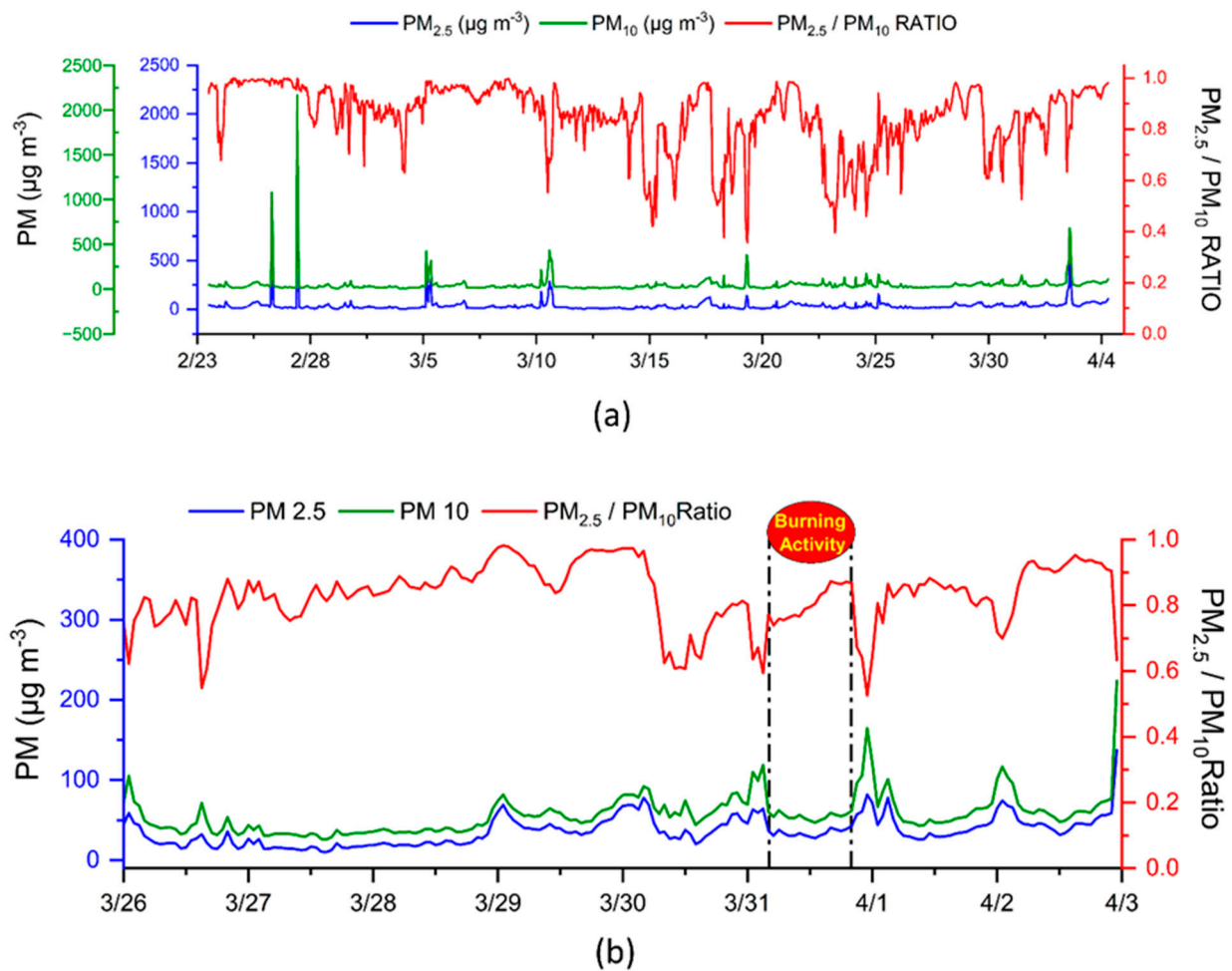


Figure 13. $\text{PM}_{2.5}/\text{PM}_{10}$ ratio plots along with $\text{PM}_{2.5}$ and PM_{10} concentrations for (a) study period and (b) the week of activity.

The mean measurements for different wavelengths are $0.63 \pm 1.61 \mu\text{g m}^{-3}$, $0.60 \pm 1.32 \mu\text{g m}^{-3}$, $0.58 \pm 1.2 \mu\text{g m}^{-3}$, $0.58 \pm 1.22 \mu\text{g m}^{-3}$, and $0.59 \pm 1.22 \mu\text{g m}^{-3}$ for 375 nm, 470 nm, 528 nm, 625 nm, and 880 nm, respectively. All the values of different wavelengths reached their maximum value on 31 March 2022, the day of burning activity.

The AAE values for various sources change with respect to the wavelengths used to calculate, but different studies resulted in concluding that the AAE values for natural emissaries are close to one, while the value of biomass burning goes up to two [33–35]. A study in Italy estimated that the AAE value ranged between 0.9–1.0 and 1.8–2.2 for fossil fuels and biomass burning, respectively [36]. Of all the different wavelength pairs possible, the pair of 370 nm and 880 nm is proven to be the most efficient pair for the estimation of BC source [36–38]. Additionally, the same has been used in this study to calculate the AAE. The mass absorption efficiencies for the 375nm, 470 nm, 528 nm, 625 nm, and 880 nm are $24.069 \text{ m}^2 \text{ g}^{-1}$, $19.070 \text{ m}^2 \text{ g}^{-1}$, $17.070 \text{ m}^2 \text{ g}^{-1}$, $14.091 \text{ m}^2 \text{ g}^{-1}$, and $10.120 \text{ m}^2 \text{ g}^{-1}$, respectively [39]. The absorption coefficient is calculated using the following equation:

$$\alpha_{abs,\lambda} = C_{BC,\lambda} \times (MAE_{BC,\lambda} \div f) \times 10^{-3}$$

$C_{BC,\lambda}$ is the measured value by the microAeth[®] MA200, $MAE_{BC,\lambda}$ is the mass absorption efficiencies, and f is the calibration factor which is assumed to be 1.3 [39]. The AAE were calculated using the following equation [40]:

$$AAE_{375/880} = - \frac{\ln(\alpha_{abs}(375nm)/\alpha_{abs}(880nm))}{\ln(375/880)}$$

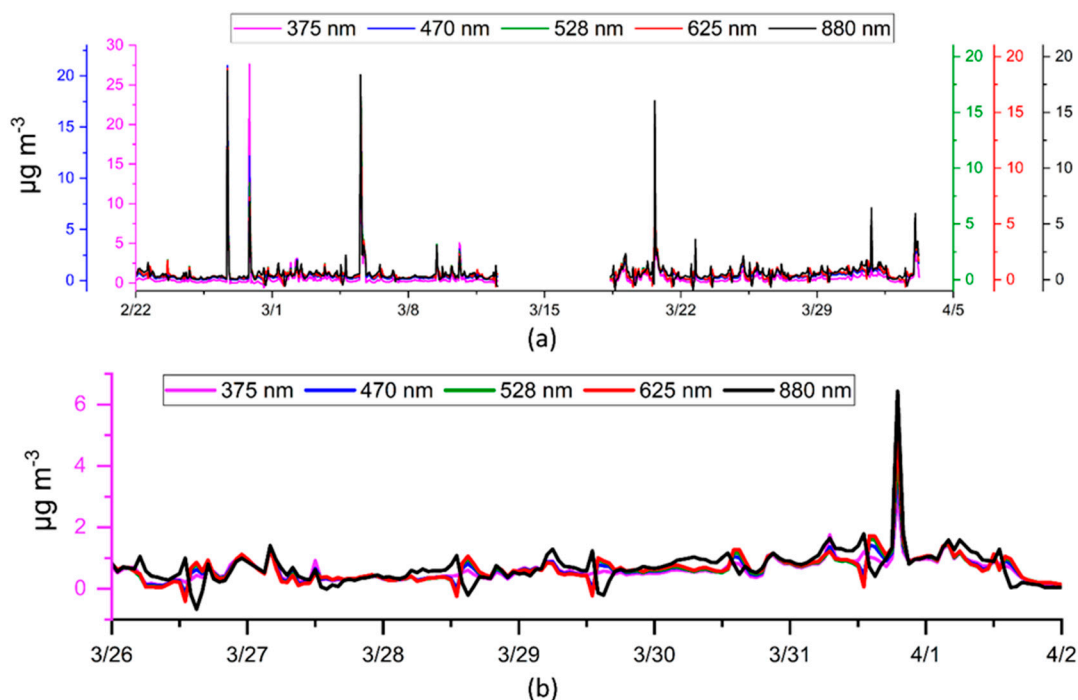


Figure 14. Measured values of different wavelengths concentration for (a) study period and (b) the week of activity.

Figure 15a shows the AAE values for the whole study period.. The mean value of Angstrom exponent for the whole study period is 0.92 ± 0.82 . The value of 0.92 ± 0.82 suggests that most of the time, the source of aerosols is natural. Diurnal patterns were observed in the AAE values. Previous studies [41,42] also concluded that AAE follows both diurnal and seasonal patterns. There are some days on which the AAE value has gone to negative. Various studies have proven that the value of AAE declines with the increase in the diameter of the Black Carbon core [43,44].

Figure 15b shows the exponent values on the day of burning activity. The value was 0.8 at the start of the day, 1.09 at 6:00 a.m., increased to 2.03 by 14:00 p.m., and dropped back to 0.17 by the 18:00 p.m. Additionally, the AAE value is 0.8 again by the end of the day. The value increased during the burning activity and decreased after it. This implies that AAE values are indicative of biomass burning and the straw burning of sugarcane causes an increase in AAE value up to 2.03.

The ratio of $PM_{2.5}$ and PM_{10} evaluated the release of particulate matter as being natural or anthropogenic, whereas the AAE used the black carbon values to help in estimating the source of aerosols. In this study, the relation between these two also has been presented. Figure 16 represents the scatter plot showing the relation between ratio of $PM_{2.5}$ to PM_{10} and absorption Ångström exponent.

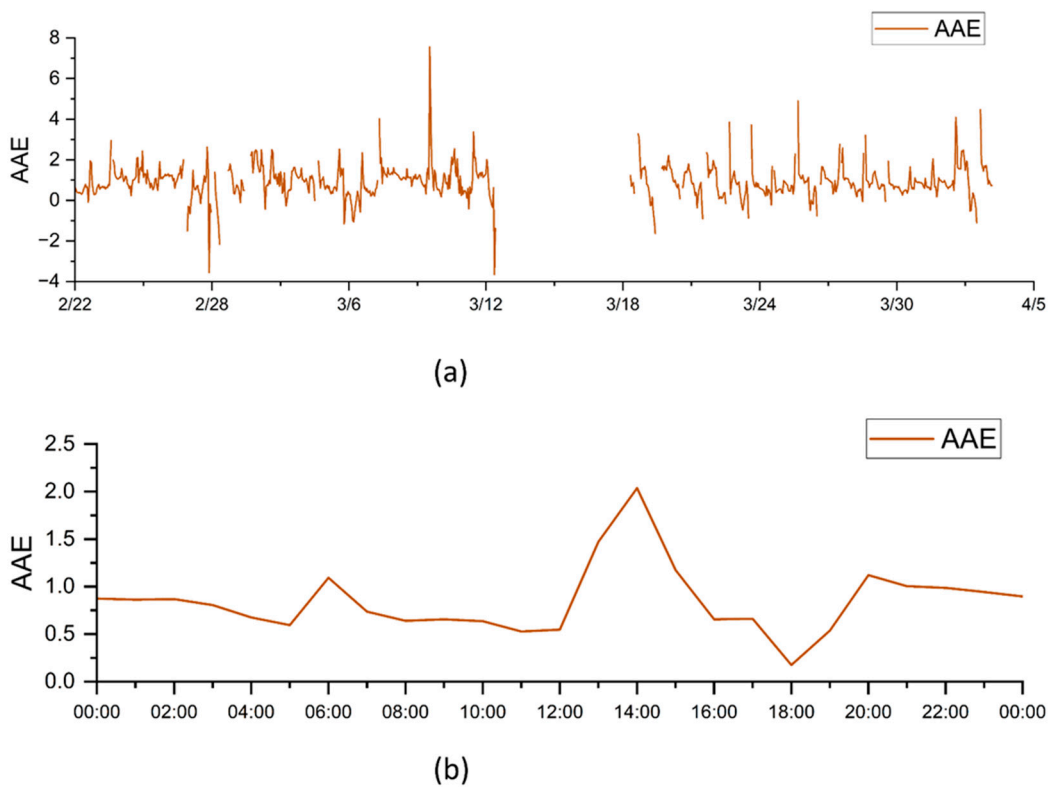


Figure 15. AAE values of the site for (a) study period (b) the day of activity.

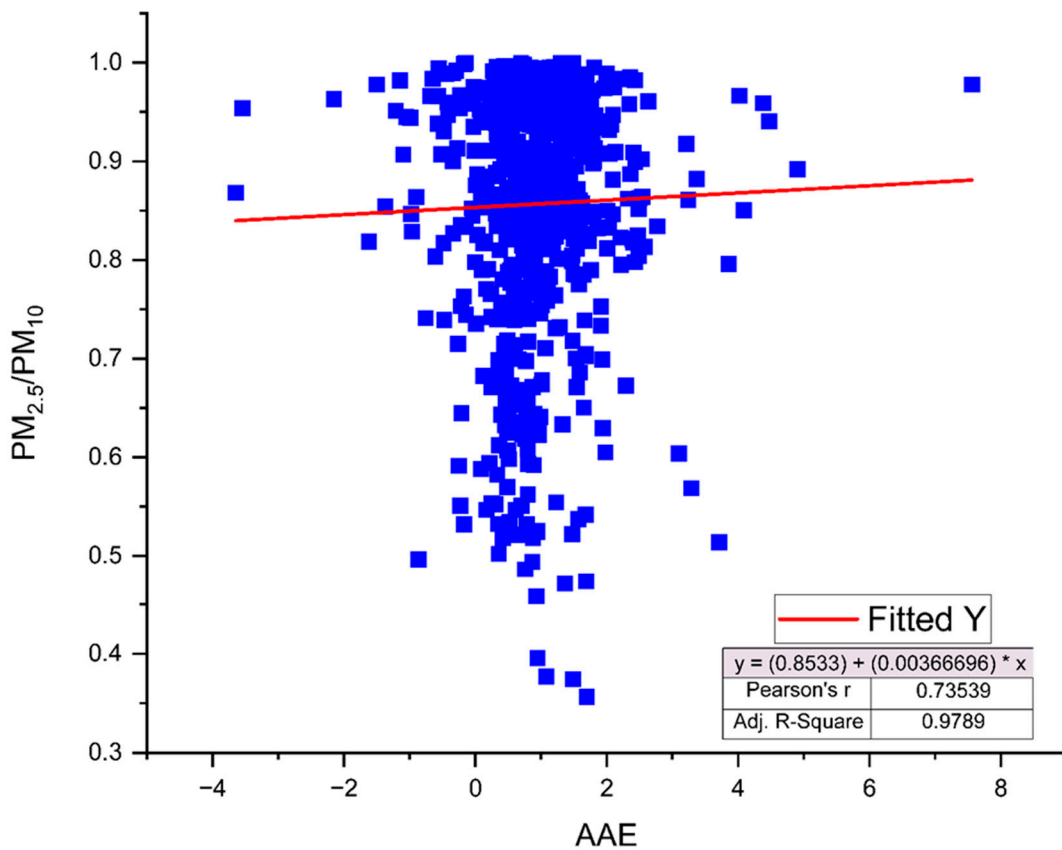


Figure 16. The regression curve of PM_{2.5} to PM₁₀ ratio and AAE.

The correlation coefficient for the plot is $R^2 = 0.97$, which indicates strong correlation between both values. The corresponding regression equation is $y = (0.8533) + (0.00366696) * x$. The Pearson correlation coefficient is 0.73, which implies strong correlation between the $PM_{2.5}$ to PM_{10} ratio and AAE.

This also indicates that either the AAE value or the $PM_{2.5}$ to PM_{10} ratio can be very useful in detecting burning activities across places, and the methods above can be followed to obtain the values from the measured concentrations.

4. Discussion and Conclusions

The Texas Open burning rules and regulations [45] state that crop residue can be burnt for agricultural management purposes if and only if there is no practical alternative. However, even though there are other methods [3] available because the method of stubble burning is considered a more economically friendly and time-saving process to eliminate crop residue, it is most widely practiced. The number of times a farm goes under stubble burn in a year depends upon the number of crops being grown on the farm. Figure 17 shows the fire activity in the southern part of Texas from November 2021 to October 2022 using the NASA's Fire Information for Resource Management System (FIRMS) US/CANADA, part of NASA's Earth Observing System Data and Information System (EOSDIS), accessed on 14 November 2022 [27]. There was a higher number of fire activities observed in the months of February (Figure 17d) and March (Figure 17e) in the area compared to others, which is the season of pre-harvesting. Even though there are several fires observed in other parts of the year, they are not as alarming as the fires in the month of February and March. Additionally, these fires need to be controlled in order to keep the air quality below required parameters.

The results of this study confirm that there is an increase in particulate matter levels and black carbon levels during the period of stubble burning. Primarily, there is a steeper increase in PM_{10} levels than in other particulate matter concentrations. Exposure to higher PM_{10} concentrations leads to long-term and short-term health effects [26]. Black carbon concentrations increased by 55% in the burning period when compared to the mean concentration of the study period. This has the potential to have deleterious health effects on humans by causing respiratory, cardiovascular diseases, and birth defects. In addition, high levels of black carbon also contribute to climate change because of its ability to absorb light as heat [46]. Carbon monoxide concentrations, which increased by 67% during the burning activity compared to the mean concentrations, are a toxic gas that reduces the oxygen delivery to the human body organs and also helps in the formation of ground-level ozone [9]. It is also proven in this study that the $PM_{2.5}$ to PM_{10} ratio and AAE values are equally important in figuring out the source of particulate matter and aerosols. The ratio of $PM_{2.5}$ to PM_{10} reached 0.87, and the AAE value reached 2.03 during the burning effect. These values can be used for source apportionment studies in the future, thus helping in differentiating between the natural and anthropogenic sources of particulate matter in studies involving larger areas.

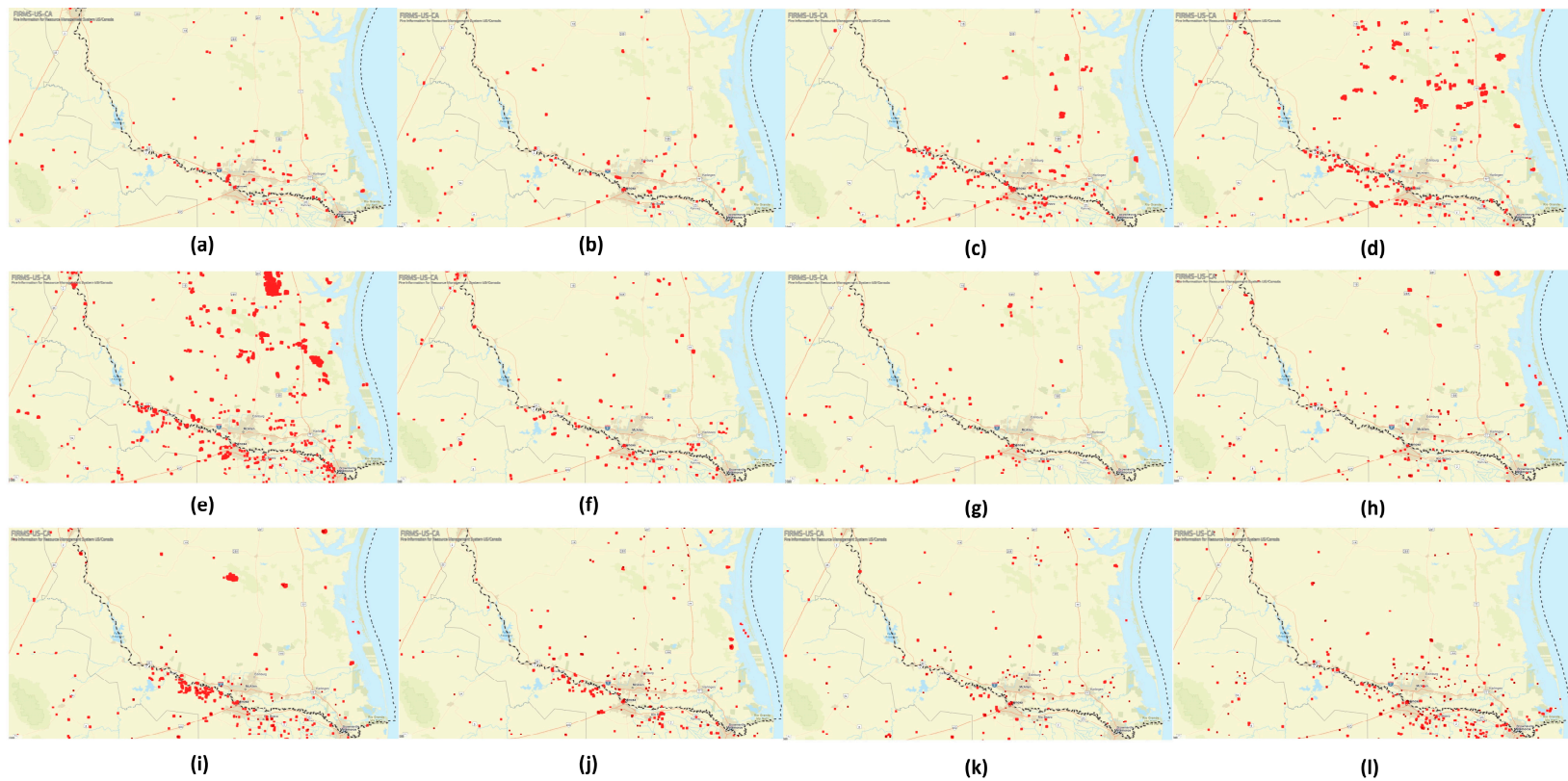


Figure 17. Fire activities in southern part of Texas in different months (a) November 2021, (b) December 2021, (c) January 2022, (d) February 2022, (e) March 2022, (f) April 2022, (g) May 2022, (h) June 2022, (i) July 2022, (j) August 2022, (k) September 2022, and (l) October 2022.

It is also important to note that urban or rural landscapes with an overall higher percentage of agricultural farms should be continuously monitored for air quality levels. Being one of the largest producers of sugarcane in the USA, the Lower Rio Grande Valley merits such air monitoring campaigns. As per our knowledge, this study is one of the first to discuss the effect of stubble burning of sugarcane on air quality in this region. At present, there are only five CAMS stations monitoring the air quality across the Lower Rio Grande Valley, out of which some are not continuously functional. Measuring the air quality at more CAMS sites would help in making better decisions regarding open-air stubble burning. With the growth in technology, there are various methods available, such as using LCS—Low-Cost Sensors to measure the air quality parameters at the neighborhood level. It has been proven that low-cost sensors are very efficient in assessing finer changes in particulate matter concentrations [7]. Therefore, it would be prudent to mention here that future research in this region should consider using LCS to characterize air pollution levels at various sites in this agricultural-intensive region of South Texas.

Author Contributions: A.U.R. conceived and designed this study; E.R. and E.M. implemented this study and supervised the data collection; S.D.P. analyzed the data and wrote the initial draft of the manuscript; A.U.R. edited and prepared the final draft. All authors provided valuable comments and ideas when drafting the manuscript. All authors have read and agreed to the published version of the manuscript.

Funding: Funding for this research work was kindly provided by the UTRGV under the new faculty startup funds given to A.U.R.

Institutional Review Board Statement: Not applicable.

Informed Consent Statement: Not applicable.

Data Availability Statement: Data is available upon request.

Acknowledgments: The authors express their gratitude to Rolando Robles for providing the space to install the air-quality instruments for the whole study period. We acknowledge the use of data and/or imagery from NASA's Fire Information for Resource Management System (FIRMS) (<https://earthdata.nasa.gov/firms>), part of NASA's Earth Observing System Data and Information System (EOSDIS), accessed on 14 November 2022.

Conflicts of Interest: The authors declare no conflict of interest.

Abbreviations

PM ₁	Particulate Matter of size less than 1 micron
PM _{2.5}	Particulate Matter of size less than 2.5 microns
PM ₁₀	Particulate Matter of size less than 10 microns
VOCs	Volatile organic compounds
CO	Carbon monoxide
NO ₂	Nitrogen dioxide
BC	Black carbon
O ₃	Ozone
NH ₃	Ammonia
SO ₂	Sulfur dioxide
NO _x	Oxides of nitrogen
NO	Nitric oxide
CO ₂	Carbon dioxide
EPA	Environmental Protection Agency
STRV	Short Tons, Raw Value
N ₂ O	Nitrous oxide
TCEQ	Texas Commission on Environmental Quality
CAMS	Continuous ambient monitoring station
COD	Coefficient of Divergence
RGV	Rio Grande Valley

FIRMS	Fire Information for Resource Management System
NASA	The National Aeronautics and Space Administration
USDA	The United States Department of Agriculture
MODIS	Moderate Resolution Imaging Spectroradiometer
VIIRS	Visible Infrared Imaging Radiometer Suite
AAE	The Absorption Ångström exponent
UVPM	Ultraviolet particulate matter
LCS	Low-Cost Sensors

References

- McCarty, J.L.; Korontzi, S.; Justice, C.O.; Loboda, T. The spatial and temporal distribution of crop residue burning in the contiguous United States. *Sci. Total Environ.* **2009**, *407*, 5701–5712. [[CrossRef](#)] [[PubMed](#)]
- Abdurrahman, M.I.; Chaki, S.; Saini, G. Stubble burning: Effects on health & environment, regulations and management practices. *Environ. Adv.* **2020**, *2*, 100011. [[CrossRef](#)]
- Kumar, P.; Joshi, L. Pollution Caused by Agricultural Waste Burning and Possible Alternate Uses of Crop Stubble: A Case Study of Punjab. In *Knowledge Systems of Societies for Adaptation and Mitigation of Impacts of Climate Change. Environmental Science and Engineering*; Springer: Berlin/Heidelberg, Germany, 2013; pp. 367–385. [[CrossRef](#)]
- Kaushal, L.A. Field Crop Residue burning Induced Particulate Pollution in NW India—Policy Challenges & Way Forward. *IOP Conf. Ser. Earth Environ. Sci.* **2022**, *1009*, 012006. [[CrossRef](#)]
- Yakupoglu, T.; Dindaroglu, T.; Rodrigo-Comino, J.; Cerdà, A. Stubble burning and wildfires in Turkey considering the Sustainable Development Goals of the United Nations. *Eurasian J. Soil Sci.* **2022**, *11*, 66–76. [[CrossRef](#)]
- Shi, T.; Liu, Y.; Zhang, L.; Hao, L.; Gao, Z. Burning in agricultural landscapes: An emerging natural and human issue in China. *Landsc. Ecol.* **2014**, *29*, 1785–1798. [[CrossRef](#)]
- Mendez, E.; Temby, O.; Wladyka, D.; Sepielak, K.; Raysoni, A.U. Fine Particulate Matter Concentrations during Independence Day Fireworks Display in the Lower Rio Grande Valley Region, South Texas, USA. *Sci. World J.* **2022**, *2022*, 8413574. [[CrossRef](#)]
- Wyer, K.E.; Kelleghan, D.B.; Blanes-Vidal, V.; Schaubberger, G.; Curran, T.P. Ammonia emissions from agriculture and their contribution to fine particulate matter: A review of implications for human health. *J. Environ. Manag.* **2022**, *323*, 116285. [[CrossRef](#)]
- Latest Findings on National Air Quality: 1997 Status and Trends. 1998. Available online: https://www.epa.gov/sites/default/files/2017-11/documents/trends_brochure_1997.pdf (accessed on 10 October 2022).
- US EPA; OAR. Carbon Monoxide's Impact on Indoor Air Quality. 2014. Available online: <https://www.epa.gov/indoor-air-quality-iaq/carbon-monoxides-impact-indoor-air-quality> (accessed on 10 October 2022).
- US EPA. Sulfur Dioxide Basics. Available online: <https://www.epa.gov/so2-pollution/sulfur-dioxide-basics> (accessed on 14 August 2020).
- Gerstenzang, J. Transportation and Global Warming. Biologicaldiversity.org. 2009. Available online: https://www.biologicaldiversity.org/programs/climate_law_institute/transportation_and_global_warming/ (accessed on 17 November 2022).
- Arunrat, N.; Pumijumngong, N.; Sereenonchai, S. Air-Pollutant Emissions from Agricultural Burning in Mae Chaem Basin, Chiang Mai Province, Thailand. *Atmosphere* **2018**, *9*, 145. [[CrossRef](#)]
- Satpathy, P.; Pradhan, C. Biogas as an alternative to stubble burning in India. *Biomass Convers. Biorefinery* **2020**, *13*, 31–42. [[CrossRef](#)]
- NAAS. *Innovative Viable Solution to Rice Residue Burning in Rice-Wheat Cropping System through Concurrent Use of Super Straw Management System-Fitted Combines and Turbo Happy Seeder. Policy Brief No. 2*; National Academy of Agricultural Sciences: New Delhi, India, 2017; p. 16.
- USDA. National Agricultural Statistics Service. Farms and Land in Farms. 2019 Summary. 2020. Available online: https://www.nass.usda.gov/Publications/Todays_Reports/reports/fnlo0220.pdf (accessed on 19 November 2022).
- USDA; National Agricultural Statistics Service. Crop Production 2021 Summary. 2022. Available online: <https://downloads.usda.library.cornell.edu/usda-esmis/files/k3569432s/sn00c1252/g158cj98r/cropan22.pdf> (accessed on 20 November 2022).
- Vidalina Abadam. Economic Research Service U.S. Department of Agriculture. 2021. Available online: <https://www.ers.usda.gov/topics/crops/sugar-sweeteners/background/> (accessed on 3 October 2022).
- 'Why is the Sugarcane Industry Important to Louisiana?', Louisiana State University Agricultural Center. Available online: <https://www.lsuagcenter.com/~media/system/3/6/f/2/36f2ecf632a7fcdd6c4b8d1186bdf28/pub2820sugarburn2.pdf> (accessed on 10 November 2022).
- França, D.D.A.; Longo, K.M.; Neto, T.G.S.; Santos, J.C.; Freitas, S.R.; Rudorff, B.F.T.; Cortez, E.V.; Anselmo, E.; Carvalho, J.J.A. Pre-Harvest Sugarcane Burning: Determination of Emission Factors through Laboratory Measurements. *Atmosphere* **2012**, *3*, 164–180. [[CrossRef](#)]
- Vera, J.C.; Valeiro, A.; Posse, G.; Acreche, M.M. To burn or not to burn: The question of straw burning and nitrogen fertilization effect on nitrous oxide emissions in sugarcane. *Sci. Total Environ.* **2017**, *587*, 399–406. [[CrossRef](#)]
- Wiedenfeld, R.P. Field Crops Research Effects of irrigation and N fertilizer application on sugarcane yield and quality. *Field Crops Res.* **1995**, *43*, 101–108. [[CrossRef](#)]

23. EPA; Climate Change Division. Inventory of U.S. Greenhouse Gas Emissions and Sinks: 1990–2020—Main Text. 1990. Available online: <https://www.epa.gov/ghgemissions/draft-inventory-us-greenhouse-gas-emissions> (accessed on 17 October 2022).
24. Texas Commission on Environmental Quality. Available online: <https://www.tceq.texas.gov/?msclkid=f4d9d722d06511ec8a5d9d27baa14eae> (accessed on 3 October 2022).
25. Todd, J.; Hale, A.; Pan, Y.; Tew, T.L.; Dufrene, E.O.; Duet, M.; Verdun, D.; Landry, C.; Grisham, M.P.; Kimbeng, C.; et al. Registration of ‘Ho 11-573’ sugarcane. *J. Plant Regist.* **2021**, *15*, 463–470. [[CrossRef](#)]
26. Raysoni, A.U.; Mendez, E.; Luna, A.; Collins, J. Characterization of Particulate Matter Species in an Area Impacted by Aggregate and Limestone Mining North of San Antonio, TX, USA. *Sustainability* **2022**, *14*, 4288. [[CrossRef](#)]
27. NRT VIIRS 375 m Active Fire Product VNP14IMGT Distributed from NASA FIRMS. Available online: <https://earthdata.nasa.gov/firms> (accessed on 31 October 2022). [[CrossRef](#)]
28. Fan, H.; Zhao, C.; Yang, Y.; Yang, X. Spatio-Temporal Variations of the PM_{2.5}/PM₁₀ Ratios and Its Application to Air Pollution Type Classification in China. *Front. Environ. Sci.* **2021**, *9*, 692440. [[CrossRef](#)]
29. Tian, P.; Zhang, L.; Ma, J.; Tang, K.; Xu, L.; Wang, Y.; Cao, X.; Liang, J.; Ji, Y.; Jiang, J.H.; et al. Radiative absorption enhancement of dust mixed with anthropogenic pollution over East Asia. *Atmos. Chem. Phys.* **2018**, *18*, 7815–7825. [[CrossRef](#)]
30. Fan, H.; Zhao, C.; Yang, Y. A comprehensive analysis of the spatio-temporal variation of urban air pollution in China during 2014–2018. *Atmos. Environ.* **2019**, *220*, 117066. [[CrossRef](#)]
31. Liu, C.; Chung, C.E.; Yin, Y.; Schnaiter, M. The absorption Ångström exponent of black carbon: From numerical aspects. *Atmos. Meas. Tech.* **2018**, *18*, 6259–6273. [[CrossRef](#)]
32. microAeth®MA Series MA200, MA300, MA350 Operating Manual. 2017. Available online: <https://aethlabs.com> (accessed on 18 November 2022).
33. Saturno, J.; Holanda, B.A.; Pöhlker, C.; Ditas, F.; Wang, Q.; Moran-Zuloaga, D.; Brito, J.; Carbone, S.; Cheng, Y.; Chi, X.; et al. Black and brown carbon over central Amazonia: Long-term aerosol measurements at the ATTO site. *Atmos. Chem. Phys.* **2018**, *18*, 12817–12843. [[CrossRef](#)]
34. Zhang, X.; Mao, M.; Yin, Y.; Tang, S. The absorption Ångström exponent of black carbon with brown coatings: Effects of aerosol microphysics and parameterization. *Atmos. Chem. Phys.* **2020**, *20*, 9701–9711. [[CrossRef](#)]
35. Goel, V.; Hazarika, N.; Kumar, M.; Singh, V.; Thamban, N.M.; Tripathi, S.N. Variations in Black Carbon concentration and sources during COVID-19 lockdown in Delhi. *Chemosphere* **2021**, *270*, 129435. [[CrossRef](#)] [[PubMed](#)]
36. Mousavi, A.; Sowlat, M.H.; Lovett, C.; Rauber, M.; Szidat, S.; Boffi, R.; Borgini, A.; De Marco, C.; Ruprecht, A.A.; Sioutas, C. Source apportionment of black carbon (BC) from fossil fuel and biomass burning in metropolitan Milan, Italy. *Atmos. Environ.* **2019**, *203*, 252–261. [[CrossRef](#)]
37. Dumka, U.; Kaskaoutis, D.; Tiwari, S.; Safai, P.; Attri, S.; Soni, V.; Singh, N.; Mihalopoulos, N. Assessment of biomass burning and fossil fuel contribution to black carbon concentrations in Delhi during winter. *Atmos. Environ.* **2018**, *194*, 93–109. [[CrossRef](#)]
38. Garg, S.; Chandra, B.P.; Sinha, V.; Sarda-Esteve, R.; Gros, V.; Sinha, B. Limitation of the Use of the Absorption Ångström Exponent for Source Apportionment of Equivalent Black Carbon: A Case Study from the North West Indo-Gangetic Plain. *Environ. Sci. Technol.* **2015**, *50*, 814–824. [[CrossRef](#)]
39. Li, C.; Windwer, E.; Fang, Z.; Nissenbaum, D.; Rudich, Y. Correcting micro-aethalometer absorption measurements for brown carbon aerosol. *Sci. Total Environ.* **2021**, *777*, 146143. [[CrossRef](#)]
40. Helin, A.; Virkkula, A.; Backman, J.; Pirjola, L.; Sippula, O.; Aakko-Saksa, P.; Väätäinen, S.; Mylläri, F.; Järvinen, A.; Bloss, M.; et al. Variation of Absorption Ångström Exponent in Aerosols From Different Emission Sources. *J. Geophys. Res. Atmos.* **2021**, *126*, e2020JD034094. [[CrossRef](#)]
41. DeWitt, H.L.; Gasore, J.; Rupakheti, M.; Potter, K.E.; Prinn, R.G.; Ndikubwimana, J.D.D.; Nkusi, J.; Safari, B. Seasonal and diurnal variability in O₃, black carbon, and CO measured at the Rwanda Climate Observatory. *Atmos. Chem. Phys.* **2019**, *19*, 2063–2078. [[CrossRef](#)]
42. Martinsson, J.; Azeem, H.A.; Sporre, M.K.; Bergström, R.; Ahlberg, E.; Öström, E.; Kristensson, A.; Swietlicki, E.; Stenström, K.E. Carbonaceous aerosol source apportionment using the Aethalometer model—Evaluation by radiocarbon and levoglucosan analysis at a rural background site in southern Sweden. *Atmos. Chem. Phys.* **2017**, *17*, 4265–4281. [[CrossRef](#)]
43. Lack, D.A.; Cappa, C.D. Impact of brown and clear carbon on light absorption enhancement, single scatter albedo and absorption wavelength dependence of black carbon. *Atmos. Chem. Phys.* **2010**, *10*, 4207–4220. [[CrossRef](#)]
44. Virkkula, A. Modeled source apportionment of black carbon particles coated with a light-scattering shell. *Atmos. Meas. Tech.* **2021**, *14*, 3707–3719. [[CrossRef](#)]
45. Treadwell, M.; Lashmet, T.D. Texas Open Burning Rules and Regulations. 2016. Available online: <https://www.epa.gov/criteria-air-pollutants/naaqs-table#1> (accessed on 22 October 2022).
46. EPA; Office of the Assistant Administrator. Black Carbon Research and Future Strategies: Reducing Emissions, Improving Human Health, and Taking Action on Climate Change. Available online: <http://www.epa.gov/research/sciencematters/august> (accessed on 29 November 2022).

Disclaimer/Publisher’s Note: The statements, opinions and data contained in all publications are solely those of the individual author(s) and contributor(s) and not of MDPI and/or the editor(s). MDPI and/or the editor(s) disclaim responsibility for any injury to people or property resulting from any ideas, methods, instructions or products referred to in the content.